Long-Term Infrasonic Monitoring of Land and Marine-Terminating Glaciers in Greenland

Evers, L. G.; Smets, P. S.M.; Assink, J. D.; Shani-Kadmiel, S.; Kondo, K.; Sugiyama, S.

DOI
10.1029/2021GL097113

Publication date
2022

Document Version
Final published version

Published in
Geophysical Research Letters

Geophysical Research Letters

RESEARCH LETTER
10.1029/2021GL097113

Long-Term Infrasonic Monitoring of Land and Marine-Terminating Glaciers in Greenland

L. G. Evers[1,2], P. S. M. Smets[2], J. D. Assink[1], S. Shani-Kadmiel[1], K. Kondo[3,4], and S. Sugiyama[4]

[1]R&D Department of Seismology and Acoustics, Royal Netherlands Meteorological Institute (KNMI), De Bilt, The Netherlands, [2]Department of Geoscience and Engineering, Faculty of Civil Engineering and Geosciences, Delft University of Technology, Delft, The Netherlands, [3]Graduate School of Environmental Science, Hokkaido University, Sapporo, Japan, [4]Institute of Low Temperature Science, Hokkaido University, Sapporo, Japan

Key Points:

- Infrasound monitoring of multiple glaciers simultaneously revealed details on glacier dynamics with a high temporal and spatial scale
- Inter-yearly to daily variations for marine (calving) and land-terminating glaciers (melt water run-off) were observedover 18 years
- Infrasound activity related to glacier discharge was highest in recent years, supported by both modeling and actual discharge measurements

Supporting Information:

Supporting Information may be found in the online version of this article.

Correspondence to:

L. G. Evers,
evers@knmi.nl

Citation:

Evers, L. G., Smets, P. S. M., Assink, J. D., Shani-Kadmiel, S., Kondo, K., & Sugiyama, S. (2022). Long-term infrasonic monitoring of land and marine-terminating glaciers in Greenland. *Geophysical Research Letters*, *49*, e2021GL097113. https://doi.org/10.1029/2021GL097113

Received 2 DEC 2021
Accepted 4 APR 2022

Author Contributions:

Conceptualization: L. G. Evers
Data curation: L. G. Evers, P. S. M. Smets
Formal analysis: L. G. Evers, P. S. M. Smets
Funding acquisition: L. G. Evers
Investigation: L. G. Evers, P. S. M. Smets, J. D. Assink, S. Shani-Kadmiel, K. Kondo, S. Sugiyama
Methodology: L. G. Evers, P. S. M. Smets, J. D. Assink, S. Shani-Kadmiel, K. Kondo, S. Sugiyama

Abstract A period of 18 years of infrasonic recordings was analyzed from a microbarometer array (I18DK) in northwestern Greenland, near Qaanaaq. A huge number of infrasonic detections, over 700,000, have been made in I18DKs soundscape during the Arctic summers. Simultaneously identified were both calving events from marine-terminating glaciers and discharge related acoustics from a land-terminating glacier. This infrasonic activity is correlated to sea-surface and atmospheric temperature, respectively. Inter-yearly to daily variations were retrieved showing a strong variability in infrasonic detection rates and hence glacier activity. The highest number of infrasonic detections were found in recent years from the land-terminating glacier. The latter is supported by actual discharge measurements and partly by a discharge model. It is concluded that monitoring infrasound from glaciers can complement other techniques to remotely and passively get insights into glacier dynamics with high temporal and spatial resolution.

Plain Language Summary Infrasound is inaudible sound and created when large volumes of air are displaced in the atmosphere. Such infrasound is continuously measured in northwestern Greenland, near the village of Qaanaaq. Recordings over 18 years have been analyzed. Both land and marine-terminating glaciers were identified, being active at the same time. Variations in activity of the glaciers were found between different years and also on a daily basis. The activity is related to calving of pieces of ice from the glacier and material running off the glacier. In recent years, the highest activity in discharge was observed. The latter is support by modeling and measurements of discharge which have been taken locally over 3 years. It is concluded, that infrasound measurements can help in gaining more insights into glacier dynamics, with high temporal and spatial resolution. As such, the detection and identification of inaudible sound complements other (remote) monitoring techniques.

1. Introduction

The displacement of large volumes of air leads to low-frequency acoustic waves in the atmosphere. This so-called infrasound is inaudible to humans as it has frequencies lower than 20 Hz. Infrasound measurements are conducted as a verification technique for the Comprehensive Nuclear-Test-Ban Treaty (CTBT) in order to detect nuclear test explosions. A world wide network of 60 infrasound arrays is being constructed as part of the International Monitoring System (IMS) (Dahlman et al., 2009). Currently, 53 arrays are certified and sending continuous recordings to the International Data Center (IDC) in Vienna (status of November 2021).

I18DK is one of the operational International Monitoring System (IMS) infrasound arrays. It consists of eight microbarometers and is situated in northwestern Greenland near the town of Qaanaaq (see Figure 1). Infrasonic recordings of I18DK are available from the International Data Center (IDC) from early 2004 up to the present date. In order to reduce the noise levels caused by wind, each microbarometer is equipped with an analog noise reducer (Hedlin & Alcoverro, 2005). At I18DK, a configuration of metal pipes with discrete inlets has been applied.

Infrasound measurements from I18DK have been previously used in studies: to passively probe sudden stratospheric warming events (Evers & Siegmund, 2009; Smets & Evers, 2014), to assess the performance of the International Monitoring System (IMS) (Le Pichon et al., 2009), in detecting the 2010 Eyjafjallajökull eruption

Project Administration: L. G. Evers
Resources: L. G. Evers
Software: L. G. Evers, P. S. M. Smets, J. D. Assink, S. Shani-Kadmiel
Supervision: L. G. Evers
Validation: L. G. Evers, P. S. M. Smets, J. D. Assink, S. Shani-Kadmiel, K. Kondo, S. Sugiyama
Visualization: L. G. Evers, J. D. Assink
Writing – original draft: L. G. Evers
Writing – review & editing: L. G. Evers, P. S. M. Smets, J. D. Assink, S. Shani-Kadmiel, K. Kondo, S. Sugiyama

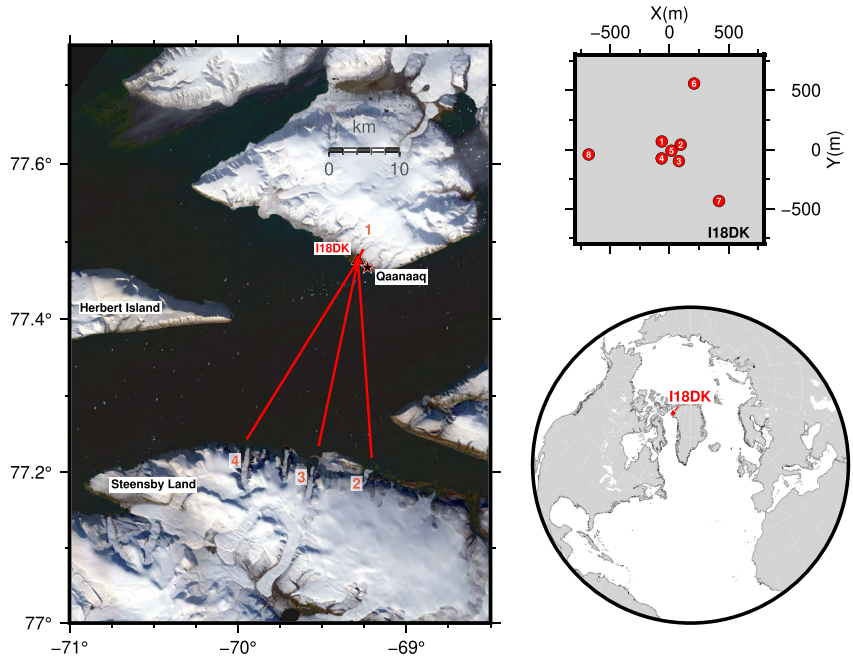

Figure 1. Maps showing the location of International Monitoring System infrasound I18DK near the city of Qaanaaq in northwestern Greenland. I18DK is configured with eight microbarometers in an array with an aperture of ~1,000 m. In the background, a Landsat 8 scene is shown of 09 September 2021 (Roy et al., 2014). The red lines indicate the retrieved back azimuths from infrasound array analysis. The back azimuth labeled with number 1 points to the Qaanaaq glacier, its land-terminating tongue is situated 2 km to the northeast of I18DK (at 25°). The marine-terminating glaciers (2–4) are located on Steensby Land to the south of I18DK (at ~30 km, between 175 and 210°). Herbert Island lies to the west of I18DK in the bay at ~25 km.

(Green et al., 2012; Matoza et al., 2011), to quantify the effect of inter-array altitude variations (Edwards & Green, 2012) and for the yield estimation of the 2013 Chelyabinsk fireball (Brown et al., 2013).

In this study, it will be shown that I18DK is capable of detecting infrasound from nearby land and marine-terminating glaciers during 18 summer seasons, starting in 2004. Source mechanisms are likely related to calving and discharge.

Calving related acoustic signals have also been identified at the Bering glacier in Alaska (Richardson et al., 2010, 2012). Murayama et al. (2017) have shown examples of infrasonic signals in the Antarctic cryosphere from: ice quakes, discharge and calving events.

Podolskiy et al. (2017) monitored the Bowdoin Glacier, near I18DK, with infrasound and identified signals related to calving, ice chasm and run-off in a river from a terminus. The latter was observed at the nearby Mirror Glacier, however, both glaciers are acoustically blocked for I18DK due to topography.

Here, inter-annual, seasonal and daily variations in glacier activity will be discussed as derived from the continuous infrasonic recordings at I18DK. The infrasonic activity will be compared to discharge measurements, modeled discharges and specifications of oceanic and atmospheric temperature.

2. Infrasound Processing and Results

Events of interest in array recordings with N instruments can be detected based on the correlation of the associated signals. Melton and Bailey (1957) proposed a so-called Fisher detector. The resulting Fisher ratio (F) is obtained by evaluating both the statistical variances in the individual recordings and the variances between the recordings. F is a measure of the signal-to-noise ratio (SNR) of the array recordings, following: $F = N \cdot SNR^2 + 1$. In this study, F was evaluated through beamforming on time-windowed recordings and by setting a detection threshold of $SNR = 1$. This array processing approach has been earlier described in, for example, Evers (2008). Prior to beamforming and detection, the detrended recordings were band-pass filtered with a second-order Butterworth

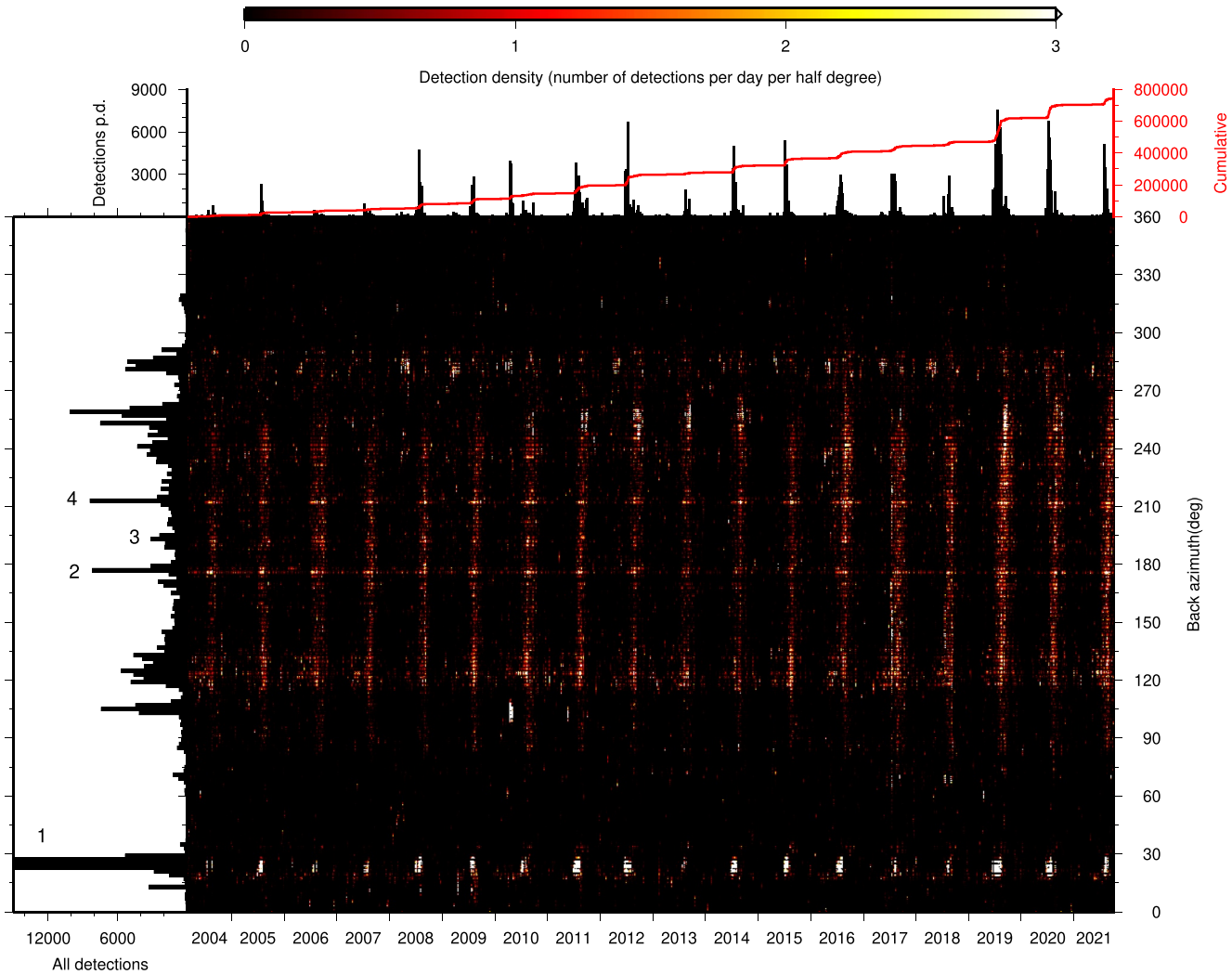

Figure 2. Infrasound detections from I18DK (Greenland) over 18 years of recordings. The detection density is shown as function of back azimuth (degrees) and time (years) from 2004 to 2021. The color coded detection density is the number of detections summed per day and half a degree in back azimuth (chosen such for plotting purposes). The back azimuth is the direction of arrival of the detection, where 0° means a source to the north of I18DK and 90° for a source to the east. Histograms with the number of detections are given to the left and on top of the main frame. The histogram to the left follows from a summation (along the horizontal) of the detections over all years, binned per two degrees in back azimuth. For plotting purposes the maximum is limited to 15,000; the actual maximum of the peak labeled as 1 is 226,386 detections. The distinct peaks in back azimuth labeled as 1–4 are also plotted in Figure 1. The top histogram is the result of (along the vertical) summing the number of detections per day. The red line within this histogram is the cumulative number of detections.

filter with corner frequencies of 1.0 and 5.0 Hz. Array processing was done on windows of 12.8s with 50% overlap. As shown in Figure 1, $N = 8$ for I18DK, however, not all eight microbarometer recordings were continuously available, due to gaps in the data. Therefore, $N \geq 7$ was chosen in the processing to guarantee a consistent image of the infrasonic soundscape surrounding I18DK over 18 years. This consistency is further assessed by analyzing the detection rate at $SNR = 1$. No significant changes or trends were found in the signal-to-noise ratio (SNR) over time, which might have indicated sudden or gradual changes in the systems response.

Figure 2 shows the soundscape resulting from array processing for the period 27 February 2004–05 October 2021. The detection density is presented as a function of the retrieved back azimuth, which is the direction-of-arrival of a signal with respect to the north. The detection density is calculated by summing the number of detections per day, per half a degree in back azimuth. Both vertical and horizontal bands of high detection densities can be seen in Figure 2. The vertical bands correspond to detections in the total of 18 summer seasons. Hardly any detections are made in winter, while the infrasonic detections are abundant in summer. The horizontal bands represent persistent sources throughout the years from specific directions. Variations between the different years

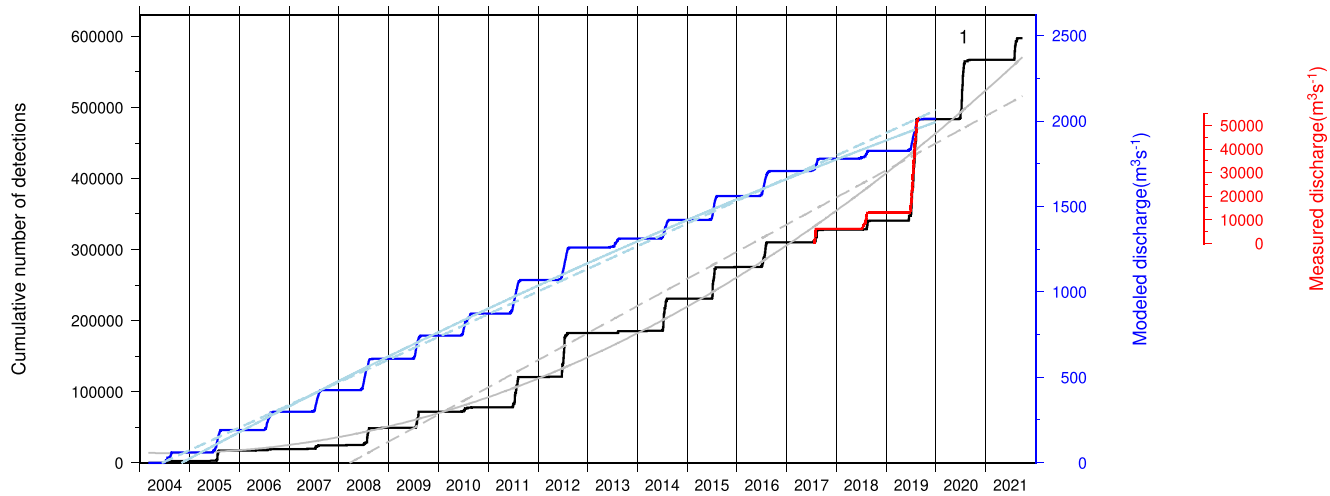

Figure 3. Infrasound detections, discharge measurements and model results for the Qaanaaq glacier. The cumulative number of infrasonic detections from the direction of the Qaanaaq glacier is shown in black. The gray dashed line represents a linear fit to the infrasound observations. The gray solid line is a quadratic polynomial fit. Discharge measurements from the Qaanaaq glacier are given in red. The blue and light blue lines follow from the Modèle Atmosphérique Régional (MAR) model and show the modeled discharge and its linear and quadratic fits. The measured and modeled discharges are scaled to the cumulative detections by aligning on the start and end time of both. The Qaanaaq glacier is indicated by the back azimuth direction 1 in Figures 1 and 2.

in source activity follow from the changes in color brightness. This is further quantified in the histogram above the detection density graph, where the number of detections per day are shown. For example, in the summer of 2012, 2019 and 2020 large numbers of detections were made, while the summers of 2004, 2006 and 2013 were infrasonically far quieter with fewer detections. From the cumulative sum in the histogram it follows that 2019 was overall the year with the most infrasonic detections. A total of 743,280 detections has been made over 18 years. To the left, the total sum of detections over the years are shown as a function of back azimuth. The persistent sources lead to distinct peaks in the histogram. Most activity appears from the northeast (~25°) with a total of 226,386 detections. At least three other peaks can be identified and labeled as 2–4, these detections have their origin to the south of I18DK.

The nature of these sources will be discussed in the next section.

3. Glacier Infrasound

A relation between ice and snow related processes in the Arctic cryosphere and the infrasonic detections is hypothesized, based on the location of I18DK in northwestern Greenland and the seasonal variations, that is, high activity in summer and low in winter. Some of the distinct back azimuths (labeled 1–4) in Figure 2 are plotted in the regional map shown in Figure 1. The back azimuth of 25° (1) points to the direction of a land-terminating tongue of the Qaanaaq glacier. Three distinct azimuths (2–4) are retrieved for southerly directions. Here, on the northern shore of Steensby Land three marine-terminating glaciers are located, between 175 and 215°. Although, a single array can not resolve distance under a plane wave assumption, it seems probable that these glaciers are the source of the infrasonic detections. Further evidence will be given by considering possible source mechanisms. In the following, the beamforming is repeated and focused on a narrow azimuthal range of 10° (for direction 1) and 5° (for 2–4) around the direction of interest.

3.1. Qaanaaq Glacier

Figure 3 shows the cumulative number of infrasonic detections as a function of time from the direction of the Qaanaaq glacier. Recall that an detection is a coherent infrasonic signal that traveled over I18DK and was made by a minimum of seven microbarometers with $SNR \geq 1$. Both years with few detections (e.g., 2006, 2010 and 2013) and years with many detections (e.g., 2012 and 2019) can be seen. The linear and quadratic fit shows that the number of detections per year is increasing over time. Especially, 2019 and 2020 have a large contribution to the increasing rate of growth.

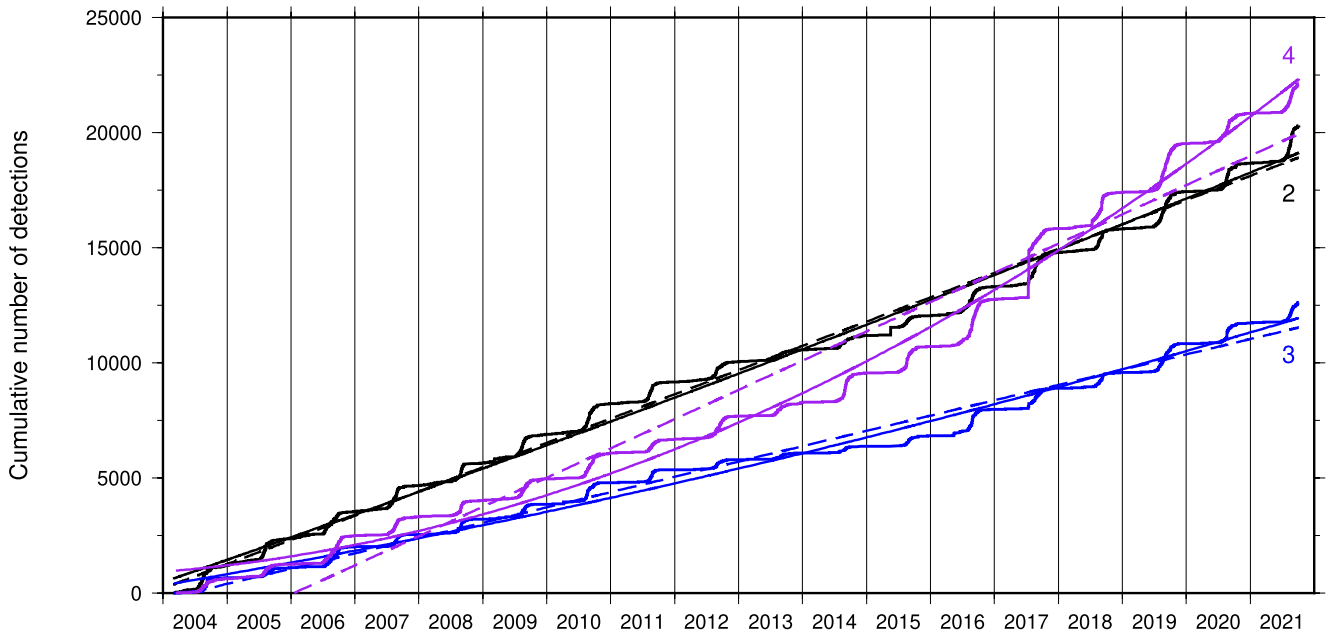

Figure 4. Infrasound detections from the direction of the marine-terminating glaciers to the south of I18DK. Shown are: the cumulative number of infrasonic detections (solid line), linear fit (straight dashed line) and quadratic fit (curved line). The sets of lines are labeled 2–4 conform the labeling in Figures 1 and 2 and indicate the different glaciers.

Discharge measurements have been conducted at the Qaanaaq glacier and are given in Figure 3 (Kondo et al., 2021). These measurements are available for 2017 up to 2019 and seem to be in correlation with the number of infrasonic detections. The length of the melt season, that is, beginning and end time, that follows from both datasets is similar. Furthermore, years with large discharges result in a high number of detections, while smaller discharge volumes lead to fewer detections.

Mankoff et al. (2020) provide discharges from the regional climate models, like the Modèle Atmosphérique Régional (MAR). These modeled discharges are also shown in Figure 3. There is a agreement between the infrasonic detections and discharge measurements and modeled values regarding the length of the melt season. On average, it lasts from the end June to the beginning of August and peaks mid-July. Years with a high number of infrasonic detections (e.g., 2012 and 2019) and years with low numbers (e.g., 2013 and 2018) also appear as years of high and low discharges in the model. However, the variability in the number of infrasound detections between 2004 and 2010 is not seen in the model.

Further correlations between the infrasonic detections and glacier discharge comes from the comparison with European Centre for Medium-Range Weather Forecasts' (ECMWF) ERA5 specifications. Figure 5a shows the average number of infrasonic detections and average atmospheric temperature (T2m) for the period 2004–2021. The European Centre for Medium-Range Weather Forecasts' (ECMWF) specifications are taken near Qaanaaq at (77.5°N, 69.25°W). There is a clear agreement between the phase and the number of the detections and temperature. An increase in temperature leads to an increase in the number of detections and vice versa. On average, both the detections and the temperature reach their maxima in July (although there is a yet unexplained difference of 2 weeks). The detections are highest early July, while the temperature reaches its maximum halfway July.

3.2. Marine-Terminating Glaciers

The directions 2–4 to the marine-terminating glaciers on Steensby Land (see Figure 1) are also individually beamformed in azimuthal ranges of 5°. The resulting cumulative number of detections are shown in Figure 4, over the period 2004–2012. Also shown are the linear and quadratic fits. In general, it follows that infrasonic detections occur in the same period, as found previously, during summer. Infrasonic activity varies for each summer, however across the 18 years a clear increase in the rate of activity over time is observed. There are short periods of intensified infrasonic activity, for example, in direction 2 in 2015 and in direction 4 in 2017. Closer

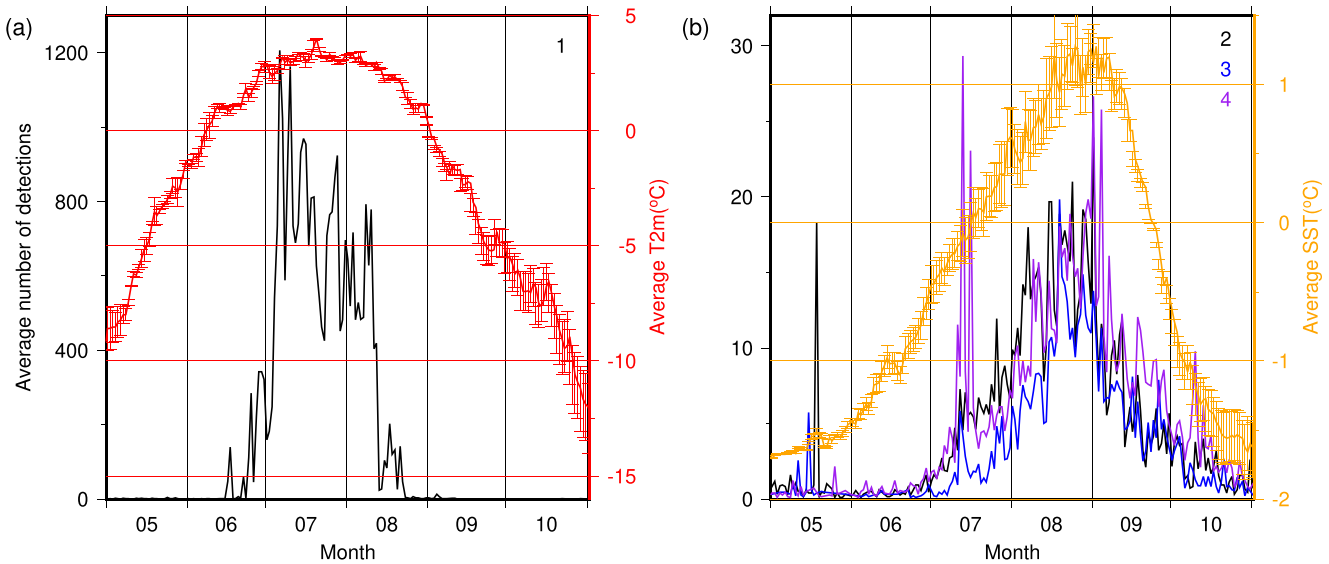

Figure 5. The European Centre for Medium-Range Weather Forecasts' (ECMWF) specifications for atmospheric temperature (a, T2m, red line) and sea-surface temperature (b, SST, orange line) are taken near Qaanaaq (77.5°N, 69.25°W). The mean values per day are averaged over the period 2004–2021. The sets of lines corresponding to the infrasonic detections are labeled 1–4 conform the labeling in earlier figures and indicate the different land and marine-terminating glaciers. The number of detections are averaged per day between 2004 and 2021. The standard deviations of the T2m and SST are also given.

inspection shows that for direction 2 the activity lasted from 18 May 2015 04:45 to 13:39 UTC, while activity from direction 4 took place between 16 July 2017 07:42 up to 09:53 UTC.

Figure 5b shows the average number of infrasonic detections and the sea-surface temperature (SST) derived from the ERA5 model for the period 2004–2021. The infrasonic activity peaks in late August/early September. This is clearly 1.5 months out of phase with the T2m, which peaks in July (Figure 5a). However, the phase and amplitude of the sea-surface temperature (SST) correlates well with the infrasonic activity, that is, the increase, decrease and peak occur at the same time. Even the shape of a slow increase and fast decrease is similar in both datasets. The distinct peaks in detections in direction 2 (May) and 4 (July) correspond to the above identified intensification in resp. 2015 and 2017.

4. Discussion

In Section 2, the soundscape surrounding I18DK (Figure 2) contains an enormous amount of infrasonic detections and hence sources. In this study, detection statistics from a few persistent back azimuths have been investigated to gain insight into the sources and source mechanisms responsible for some of the infrasonic detections. However, more interesting findings can be expected from further studying the long-term soundscape. For example, the back azimuth range 240°–270° points in the direction of Herbert Island (see Figure 1). Infrasonic activity is highly variable between the different years. A first analysis shows that the activity is in phase with the sea-surface temperature (SST). Marine-terminating glaciers on Herbert Island or sea-ice interactions with the island's shores might be sources of infrasound.

Figure 2 also shows that during the winter of 2010 a source has been temporarily active to the east of I18DK (∼104°). (Slight activity was also detected in 2011.) Another source more continuously present in winter is situated to the east at ∼282°. The nature of the sources is unknown. However, it is hypothesized that these sources have an anthropogenic origin as natural infrasound is limited in the Arctic winter.

In Section 3, the beamforming was focused on specific glaciers by only considering a narrow azimuthal range of 5° around the back azimuth of interest. This optimizes the array sensitivity to that direction, as other and possibly more coherent sources from different back azimuths can no longer be detected as coherent arrivals. In other words, the associated delay times of these signals over I18DK are no longer evaluated in the beamforming. However, the signals are still present as noise in the recordings, which reduces the signal-to-noise ratio (SNR) of the beam. This effect is equally present in all azimuthal ranges (1–4) and, therefore, does not influence the overall

findings. However, a true separation of multiple sources simultaneously active in array recordings can be realized with high-resolution beamforming (den Ouden et al., 2020).

Furthermore, in Section 3, agreement is found between the absolute values of the measured discharge and the number of infrasonic detections for the Qaanaaq glacier. This agreement is not found for the modeled values and number of detections. Furthermore, the absolute values of the measured and modeled discharges differ by a factor of 100. Possibly, the spatial resolution of the regional climatological models is too coarse to resolve atmospheric variations for the relatively small Qaanaaq Glacier (2 km wide and 7 km long). Although the model data has been downscaled to a one-km grid size Mankoff et al. (2020), the original resolution is 7.5 km for Modèle Atmosphérique Régional (MAR). The topography (e.g., elevation) of the original grid as well as the ice mask might cause such biases. A lack of long-term meteorological data in the region may also affect the accuracy of calibration and validation procedures of the regional model. The nearest weather station is in Thule, which is 100 km from the glacier. It is beyond the scope of this paper to further discuss the difference in models and measurements. The aim is to provide insight into the causal relations between glacier dynamics (i.e., discharge and calving) and infrasonic detections.

An increase in measured discharge corresponds to more detections (Section 3). In signal detection terms: the likelihood of a signal being detected in a short time window with $SNR \geq 1$ increases, when more coherent infrasound is generated due to a larger discharge. However, as shown by Marchetti et al. (2019) for debris flows, an increase in the flow rate leads to an increase in the infrasonic amplitudes but not necessarily to more coherent infrasound, that is, a higher number of detections. Of importance are the in-phase components of the infrasonic wavefield, which appeared to be connected to persistent sources. Therefore, it is hypothesized that the increase in discharge of the Qaanaaq glacier leads to more coherent infrasound (at $SNR \geq 1$) being excited by acoustic resonators like cavities and pipes. Stable sources in the river, at for example, discontinuities in topography, can further contribute by generating more coherent infrasound under an increasing discharge.

5. Concluding Remarks

Infrasonic activity around IMS station I18DK, as shown through its soundscape, has been studied for the period 2004–2021. It has been found that infrasonic activity is correlated with atmospheric and SST. Partial agreement has been found with measured and modeled glacier discharges. Based on this evidence, a causal relation between infrasonic activity and glacier dynamics is posed.

For the land-terminating Qaanaaq glacier, an increasing rate of growth in infrasonic activity over time is obtained. Discharge in the form of melt water run-off is the most probable source, which is confirmed by its relation with atmospheric temperature. Infrasound is expected to be generated by the melt water flowing over and within the glacier through channels, cavities and pipes. Furthermore, the river formed at the glaciers terminating point will generate infrasound (Podolskiy et al., 2017).

The marine-terminating glaciers on Steensby Land also show a more than linear increase over time in activity. The activity is controlled by the SST, which makes calving the expected source (Richardson et al., 2010, 2012). Hence, the Modèle Atmosphérique Régional (MAR) model is not used for comparison. The larger source-receiver distance (30 km instead of 2 km for the Qaanaaq glacier) makes the infrasonically modest process of melt water run-off less likely to be notable over such long ranges. Periods of high activity of a few hours have been identified and may corresponds to large and long-lasting calving events.

Knowledge on individual glaciers based on in-situ measurements is important for addressing the impact on the environment and society (Sugiyama et al., 2021) and for assessing long-term changes in glacier behavior (Young et al., 2022). The latter citations and references therein serve as recent examples. Here, it is found that each glacier shows a distinct behavior on the basis of the long-term infrasonic detections, which is most likely indicative for glacier-specific dynamics.

It is concluded that, infrasound measurements can serve as an independent proxy for monitoring glacier dynamics. Long-time series allow for assessing changes in relation to climate change. Multiple glaciers can be monitored simultaneously, both in the near (km) and far field (tens of km) as well as at high temporal resolution. Therefore, infrasound can complement other techniques to remotely gain information on changes in the cryosphere. Such

information is obtained by passively listening with an ear (i.e., microbarometer array) sensitive to inaudible sound and mapping its detected soundscape to the surrounding environment.

Data Availability Statement

The infrasonic detections per glaciers as a function of time are provided as Supporting Information S1 and in the 4TU. ResearchData repository under https://doi.org/10.4121/19390835. For research purposes, infrasound data from the International Monitoring System are available through the CTBTO's virtual Data Exploitation Centre (vDEC https://www.ctbto.org/specials/vdec/), through a zero-cost agreement. Data are thus freely available and can be requested online (http://www.ctbto.org/index.php?id=4701). European Centre for Medium-Range Weather Forecasts' (ECMWF) ERA5 re-analysis can be obtained from: https://www.ecmwf.int/en/forecasts/datasets/reanalysis-datasets/era5. Landsat 8 scenes are available from http://earthexplorer.usgs.gov.

Acknowledgments
The authors thank Dr. David Green for his review, which greatly helped in improving the manuscript. It takes lots of efforts to realize continuous and high-quality data sets from International Monitoring System (IMS) stations, especially for an infrasound array such as I18DK located in the Arctic. The authors thank the CTBTO and its station operators for providing these IMS recordings. The authors are grateful to Dr. E. Podolskiy from the Arctic Research Center (Hokkaido University, Japan) for bringing the Japanese and Dutch research groups together. L.E., P.S. and S.S.-K.'s contributions are funded through a VIDI project from the Netherlands Organization for Scientific Research (NWO), project 864.14.005. Figures in this letter were made with the Generic Mapping Tools (Wessel et al., 2013).

References

Brown, P. G., Assink, J. D., Astiz, L., Blaauw, R., Boslough, M. B., Borovicka, J., et al. (2013). A 500-kiloton airburst over Chelyabinsk and an enhanced hazard from small impactors. *Nature*, *503*(7475), 238–241. https://doi.org/10.1038/nature12741

Dahlman, O., Mykkeltveit, P., & Haak, H. (2009). Establishing the verification regime. In *Nuclear test ban* (pp. 1–30). https://doi.org/10.1007/978-1-4020-6885-0_6

den Ouden, O. F. C., Assink, J. D., Smets, P. S. M., Shani-Kadmiel, S., Averbuch, G., & Evers, L. G. (2020). CLEAN beamforming for the enhanced detection of multiple infrasonic sources. *Geophysical Journal International*, *221*(1), 305–317.

Edwards, W. N., & Green, D. N. (2012). Effect of interarray elevation differences on infrasound beamforming. *Geophysical Journal International*, *190*(1), 335–346. https://doi.org/10.1111/j.1365-246x.2012.05465.x

Evers, L. G. (2008). *The inaudible symphony: On the detection and source identification of atmospheric infrasound* (Unpublished doctoral dissertation). Delft University of Technology. Retrieved from http://resolver.tudelft.nl/uuid:4de38d6f-8f68-4706-bf34-4003d3dff0ce

Evers, L. G., & Siegmund, P. (2009). Infrasonic signature of the 2009 major sudden stratospheric warming. *Geophysical Research Letters*, *36*(23), 1–6. https://doi.org/10.1029/2009gl041323

Green, D. N., Matoza, R. S., Vergoz, J., & Le Pichon, A. (2012). Infrasonic propagation from the 2010 Eyjafjallajökull eruption: Investigating the influence of stratospheric solar tides. *Journal of Geophysical Research*, *117*(D21), D21202. https://doi.org/10.1029/2012jd017988

Hedlin, M. A. H., & Alcoverro, B. (2005). The use of impedance matching capillaries for reducing resonance in rosette infrasonic spatial filters. *Journal of the Acoustical Society of America*, *117*(4), 1880–1888. https://doi.org/10.1121/1.1760778

Kondo, K., Sugiyama, S., Sakakibara, D., & Fukumoto, S. (2021). Flood events caused by discharge from Qaanaaq glacier, Northwestern Greenland. *Journal of Glaciology*, *67*(263), 500–510. https://doi.org/10.1017/jog.2021.3

Le Pichon, A., Vergoz, J., Blanc, E., Guilbert, J., Ceranna, L., Evers, L., & Brachet, N. (2009). Assessing the performance of the international monitoring system's infrasound network: Geographical coverage and temporal variabilities. *Journal of Geophysical Research*, *114*(D8), 1–15. https://doi.org/10.1029/2008jd010907

Mankoff, K. D., Noël, B., Fettweis, X., Ahlstrøm, A. P., Colgan, W., Kondo, K., et al. (2020). Greenland liquid water discharge from 1958 through 2019. *Earth System Science Data*, *12*(4), 2811–2841. https://doi.org/10.5194/essd-12-2811-2020

Marchetti, E., Walter, F., Barfucci, G., Genco, R., Wenner, M., Ripepe, M., et al. (2019). Infrasound array analysis of debris flow activity and implication for early warning. *Journal of Geophysical Research*, *124*(2), 567–587. https://doi.org/10.1029/2018jf004785

Matoza, R. S., Vergoz, J., Le Pichon, A., Ceranna, L., Green, D. N., Evers, L. G., et al. (2011). Long-range acoustic observations of the Eyjafjallajökull eruption, Iceland, April-May 2010. *Geophysical Research Letters*, *38*(6), L06308. https://doi.org/10.1029/2011gl047019

Melton, B., & Bailey, L. (1957). Multiple signal correlators. *Geophysics*, *22*(3), 565–588. https://doi.org/10.1190/1.1438390

Murayama, T., Kanao, M., Yamamoto, M., & Ishihara, Y. (2017). Infrasound signals and their source location inferred from array deployment in the Lützow-Holm Bay Region, East Antarctica: January-June 2015. *International Journal of Geosciences*, *8*, 181–188. https://doi.org/10.4236/ijg.2017.82007

Podolskiy, E. A., Genco, R., Sugiyama, S., Walter, F., Funk, M., Minowa, M., & Ripepe, M. (2017). Seismic and infrasound monitoring of Bowdoin Glacier, Greenland. *Low Temperature Science*, *75*, 15–36.

Richardson, J. P., Waite, G. P., FitzGerald, K. A., & Pennington, W. D. (2010). Characteristics of seismic and acoustic signals produced by calving, Bering Glacier, Alaska. *Geophysical Research Letters*, *37*(3), L03503. https://doi.org/10.1029/2009gl041113

Richardson, J. P., Waite, G. P., Pennington, W. D., Turpening, R. M., & Robinson, J. M. (2012). Icequake locations and discrimination of source and path effects with small aperture arrays, Bering Glacier terminus, AK. *Journal of Geophysical Research*, *117*(F4), F04013. https://doi.org/10.1029/2012jf002405

Roy, D., Wulder, M., Loveland, T., Woodcock, C. E., Allen, R., Anderson, M., et al. (2014). Landsat-8: Science and product vision for terrestrial global change research. *Remote Sensing of Environment*, *145*, 154–172. https://doi.org/10.1016/j.rse.2014.02.001

Smets, P. S. M., & Evers, L. G. (2014). The life cycle of a sudden stratospheric warming from infrasonic ambient noise observations. *Journal of Geophysical Research*, *119*(21), 12084–12099. https://doi.org/10.1002/2014jd021905

Sugiyama, S., Kanna, N., Sakakibara, D., Ando, T., Asaji, I., Kondo, K., et al. (2021). Rapidly changing glaciers, ocean and coastal environments, and their impact on human society in the Qaanaaq region, northwestern Greenland. *Polar Science*, *27*, 100632. https://doi.org/10.1016/j.polar.2020.100632

Wessel, P., Smith, W. H. F., Scharroo, R., Luis, J., & Wobbe, F. (2013). Generic mapping tools: Improved version released. *Eos, Transactions American Geophysical Union*, *94*(45), 409–410. https://doi.org/10.1002/2013eo450001

Young, T. J., Christoffersen, P., Bougamont, M., Tulaczyk, S. M., Hubbard, B., Mankoff, K. D., & Stewart, C. L. (2022). Rapid basal melting of the Greenland ice sheet from surface meltwater drainage. *Proceedings of the National Academy of Sciences*, *119*(10), e2116036119. https://doi.org/10.1073/pnas.2116036119